Applied Catalysis B: Environmental 170-171 (2015) 124–134

Contents lists available at ScienceDirect

Applied Catalysis B: Environmental

journal homepage: www.elsevier.com/locate/apcatb

Protonated titanate nanotubes as a highly active catalyst for the synthesis of renewable diesel and jet fuel range alkanes

Shanshan Li[a,b], Ning Li[a,**], Guangyi Li[a], Lin Li[a], Aiqin Wang[a], Yu Cong[a], Xiaodong Wang[a], Guoliang Xu[a], Tao Zhang[a,*]

[a] State Key Laboratory of Catalysis, Dalian Institute of Chemical Physics, Chinese Academy of Sciences, Dalian 116023, PR China
[b] Graduate University of Chinese Academy of Sciences, Beijing 100049, PR China

ARTICLE INFO

Article history:
Received 5 October 2014
Received in revised form 6 December 2014
Accepted 19 January 2015
Available online 21 January 2015

Keywords:
Lignocellulose
Renewable diesel
Titanate nanotube
Hydroxyalkylation/alkylation
Hydrodeoxygenation

ABSTRACT

Protonated titanate nanotube (PTNT) was first reported as a good catalyst for the hydroxyalkylation/alkylation (HAA) of 2-methylfuran (2-MF) and *n*-butanal from lignocellulose. Compared with other inorganic solid acids, PTNT has higher catalytic activity and efficiency. Over it, high yield of HAA product (77%) was achieved under mild reaction conditions. PTNT is also effective for the HAA (or alkylation) reactions between 2-MF and other lignocellulosic carbonyl compounds. According to the characterization results, the hydrothermal treatment of TiO_2 P25 with NaOH solution and subsequent acidification significantly increases its BET surface area and the amount of acid sites on the surface of catalyst. Moreover, these pretreatments also lead to the generation of strong acid sites and Brönsted acid sites on the surface of catalyst. All of these changes are responsible for the excellent performance of PTNT. As the final aim of this work, the HAA product of 2-MF and *n*-butanal was converted to diesel and jet fuel range brached alkanes by the hydrodeoxygenation (HDO) over zeolite loaded Ni catalysts. Among them, Ni/H-ZSM-5 demonstrated the best catalytic performance and good stability, which makes it a promising catalyst in future application.

1. Introduction

With the increase of social concern about the energy and environmental problems, the catalytic conversion of renewable biomass to fuels [1–7] and chemicals [8–16] becomes a hot topic. Lignocellulose is the main component of agriculture waste and forest residues. Diesel and jet fuel are two kinds of often used transportation fuels. Pioneered by the research works of Dumesic [17–19], Corma [20–22] and Huber [23,24], the synthesis of diesel and jet fuel range alkanes with the lignocellulosic platform chemicals has attracted tremendous attention [25–31]. The synthetic strategy for the diesel and jet fuel range alkanes usually contains two steps: in the first step, diesel (C_9—C_{22}) and jet fuel (C_8—C_{16}) range oxygenates were synthesized by the C—C coupling reactions of the lignocellulosic platform chemicals. After the hydrodeoxygenation (HDO) of these oxygenates, diesel and jet fuel range alkanes can be produced.

Furfural is an important chemical which has been produced on a large scale by the hydrolysis and dehydration of hemicellulose part of agriculture waste and forest residues [32]. In the previous works of Dumesic group [17,33,34] and Huber et al. [23,24], it was found that C_8—C_{15} oxygenates can be synthesized by the aldol condensation of furfural (or 5-hydroxymethylfurfural) and acetone which can be obtained from the Acetone-*n*-Butanol–Ethanol (ABE) fermentation of lignocellulose. These oxygenates can be converted to diesel and jet fuel range straight alkanes by the hydrogenation and the HDO of hydrogenated oxygenates. In the recent work of our group [35], diesel and jet fuel range branched alkanes were obtained at high overall yield by the solvent-free aldol condensation of furfural and methyl isobutyl ketone (MIBK) followed by direct HDO.

2-methylfuran (2-MF) is a partial hydrogenation product of furfural. It was found by Corma et al. [20–22] and our group [36–39] that diesel and jet fuel range brancehd alkanes can be synthesized by the hydroxyalkylation/alkylation (HAA) of 2-MF and carbonyl compounds over acid catalysts, followed by the HDO process. Titanium is the ninth abundant element on earth. Due to its relatively low price, high availability and chemical stability, titania has been widely used as catalyst (or catalyst support). Titanate nanotube and

* Corresponding author. Tel.: +86 411 84379015; fax: +86 411 84691570.
** Corresponding author. Tel.: +86 411 84379738; fax: +86 411 84685940.
E-mail addresses: lining@dicp.ac.cn (N. Li), taozhang@dicp.ac.cn (T. Zhang).

http://dx.doi.org/10.1016/j.apcatb.2015.01.022
0926-3373/

nanowire are new materials which can be readily prepared by the hydrothermal treatment of commercial TiO_2 with NaOH solution [40–43]. During the past years, most of the works about the titanate nanotube and nanowire are concentrated on the photo-catalysis. To the best of our knowledge, there is no report about the application of titanate nanotube or nanowire for the HAA of 2-MF and lignocellulose derived carbonyl compounds.

In this work, the protonated titanate nanotube (PTNT) was first used for the HAA of 2-MF and *n*-butanal. Compared with other inorganic solid acid catalysts, the PTNT exhibited higher activity. The possibility to use the PTNT in the HAA reactions of 2-MF and other lignocellulosic carbonyl compounds was also explored. The HAA product of 2-MF and *n*-butanal was hydrodeoxygenated over a series of zeolite loaded Ni catalysts. Among them, Ni/H-ZSM-5 exhibited the best catalytic performance and good stability. To figure out the reason for the excellent performances of PTNT and Ni/H-ZSM-5, the catalysts were characterized by various technologies.

2. Experimental

2.1. Preparation of catalysts

The protonated titanate nanotube (PTNT) was prepared according to the modified method described in the literature [43]. Typically, 5.0 g commercial TiO_2 P25 (Degussa) was added to 70 mL aqueous solution of 10 mol L^{-1} NaOH. After being stirred for 10 min, the slurry was transferred to a 150 mL teflon-lined autoclave. The autoclave was put into an oven and kept at 423 K for 20 h. The solid product was filtrated from aqueous phase and washed thoroughly with large amount of water until the pH of filtrate was about 7. The sodium titanate nanotube (NaTNT) as obtained was ion-exchanged with 0.1 mol L^{-1} HNO_3 solution, filtrated, washed thoroughly with deionized water and dried at 333 K for 12 h to get the PTNT. For comparison, we also prepared the protonated layered titanate (PLT) and protonated titanate nanowire (PTNW). The PLT was synthesized by the method described in the literature [43]. TiO_2 P25 was fully mixed with Na_2CO_3 at a molar ratio of 3.0:1.1. The mixture was put in nickel crucible with a lid and calcinated at 1073 K for 18 h. After grinding, the mixture was calcinated for another 20 h to obtain the layered sodium titanate (NaLT). The NaLT was ion-exchanged with 1 mol L^{-1} HCl aqueous solution for seven days (during this period, the HCl aqueous solution was renewed daily), filtrated, washed thoroughly with water and dried at 333 K for 12 h to get the PLT. The PTNW was prepared according to the method reported by Tian et al. [44]. Typically, 0.3 g TiO_2 P25 and 40 mL, 10 mol L^{-1} NaOH aqueous solution were put into an 80 mL teflon-lined autoclave. The hydrothermal reaction was carried out at 438 K for 7 days. After being filtrated from NaOH solution and washed, the sodium titanate nanowire (NaTNW) was ion-exchanged with 0.1 mol L^{-1} HNO_3 solution, filtrated, washed thoroughly with water and dried at 333 K for 12 h to get the PTNW.

Sulfated zirconia (SO_4^{2-}/ZrO_2) was prepared according to the method described in our previous work [45] by the impregnation of $Zr(OH)_4$ with an aqueous solution of $(NH_4)_2SO_4$ (0.5 mol L^{-1}, 15 mL g_{cat}^{-1}). The slurry was stirred for 0.5 h, filtrated without washing and dried at 393 K for 12 h. Before being used for the reaction, the sulfated zirconia was calcinated in air at 923 K for 6 h. The sulfated alumina (SO_4^{2-}/Al_2O_3) was prepared according to literature [46] by the pretreatment of the γ-Al_2O_3 with an aqueous solution of H_2SO_4 (2.5 mol L^{-1}, 15 mL g_{cat}^{-1}). The mixture was stirred for 0.5 h, filtrated and dried at 393 K for 12 h. Before being used for the reaction, the sulfated alumina was calcinated in air at 873 K for 6 h. Zirconium phosphate (ZrP) was prepared according to literature [47] by mixing the 1 mol L^{-1} $ZrCl_2O{\cdot}8H_2O$ aqueous solution and the 1 mol L^{-1} $(NH_4)H_2PO_4$ aqueous solution at a volume ratio of 1:2. The precipitate was filtrated, washed with deionized water, dried at 333 K overnight and calcinated at 673 K for 4 h. H-ZSM-5 (SiO_2/Al_2O_3 = 25), H-MOR (SiO_2/Al_2O_3 = 24) and H-β (SiO_2/Al_2O_3 = 25) were provided by Nankai University.

H-ZSM-5, H-MOR and H-β loaded Ni catalysts (denoted as Ni/H-ZSM-5, Ni/H-MOR and Ni/H-β) were prepared by the incipient wetness impregnation of different zeolites with the aqueous solutions of $Ni(NO_3)_2{\cdot}6H_2O$. The SiO_2/Al_2O_3 molar ratios of H-ZSM-5, H-MOR and H-β supports were 25, 24 and 25, respectively. To facilitate the comparison, the theoretical Ni contents in different Ni catalysts were controlled as 4% by weight (denoted as 4 wt.%). After the impregnation step, the catalyst precursors were kept at room temperature overnight, dried at 333 K for 12 h, and calcinated at 773 K for 4 h. All of these Ni catalysts were reduced in-situ by H_2 flow at 773 K for 2 h before being used in the HDO process.

2.2. Characterization

2.2.1. Transmission electron microscope (TEM)

The TEM images of the titanate catalysts and the Ni catalysts were obtained with a TECNAI G^2 Spirit FEI transmission electron microscopy operated at an accelerating voltage of 120 kV. Before the tests, the Ni catalysts were reduced by H_2 at 773 K for 2 h.

2.2.2. Inductively coupled plasma-atomic emission spectrometry (ICP-AES)

The contents of titanium and sodium in the titanate catalysts were measured by ICP-AES. To do this, the PTNT, NaTNT, PTNW, NaTNW, PLT and NaLT samples were added to 25% ammonium hydroxide solution (0.01 g sample in 10 mL ammonium hydroxide solution) and stirred for 5 min, respectively. Subsequently, 30% H_2O_2 solution was added to the above mixtures and stirred until the titanates were fully dissolved. The as-obtained solutions were diluted with water. The pH values of the solutions were adjusted with HCl solution to 7. The concentrations of titanium and sodium in the samples were measured using ICP-OES (PerkinElmer Optima 7300DV). On the basis of these values, we calculated the titanium contents, sodium contents and Na/Ti atomic ratios in different titanate samples.

2.2.3. X-ray diffraction (XRD)

XRD patterns of different catalysts were recorded with a PW3040/60X′ Pert PRO (PANalytical) diffractometer using a Cu Kα radiation source (λ = 0.15432 nm) operated at 40 kV and 40 mA.

2.2.4. N_2–physical adsorption

The N_2-physical adsorption was carried out at 77 K by ASAP 2010 (micromeritics). The specific surface areas of different samples were measured by Brunauer–Emmett–Teller (BET) method. Before each measurement, the sample was evacuated at 393 K to eliminate the adsorbents.

2.2.5. NH_3 chemisorption

The amounts of acid sites on the surfaces of different solid acid catalysts and the zeolite supports were measured by NH_3 chemisorption according to the method described in our previous work [48]. The measurements were carried out by a micrometeritics autochem 2920 automated catalyst characterization system. Typically, 0.1 g of catalyst was loaded into a quartz reactor, purged at 393 K for 2 h and cooled down to 373 K in He flow. Subsequently, pulses of NH_3 (1 mL) were dosed in the reactor until saturation. The amounts of acid sites on different catalysts were calculated by the adsorptions of NH_3 during the tests.

2.2.6. NH_3 temperature programmed desorption (NH_3–TPD)

The acid strengths of titanate catalysts and the zeolite supports were characterized by NH_3–TPD which was carried out on a micrometeritics autochem II 2920 automated catalyst characterization system. For each test, 0.1 g sample was used. Before the measurement, the sample was purged with He flow at 393 K for 2 h. After saturated adsorption of NH_3 at 373 K, the sample was heated at 373 K in He flow for 45 min to remove the physically adsorbed ammonia. Desorption of NH_3 was conducted in He flow from 373 K to 1073 K at a heating rate of 10 K min^{-1}. The desorbed NH_3 molecules were detected by an OminiStar mass spectrometry (MS) equipped with the software quadstar 32-bit.

2.2.7. Fourier transform infrared spectroscopy (FT-IR)

The FT-IR spectra of different protonated titanate catalysts were collected on a Bruker Equinox 55 spectrometer equipped with a mercury–cadmium–telluride (MCT) infrared detector, a deuterated triglycine sulphate (DTGS) detector and an extended KBr beam splitter at a resolution of 4 cm^{-1}. The protonated titanate catalysts were pressed to self-supporting tablets and recorded with the DTGS detector in transmittance mode without pretreatment. From the FT-IR spectra of these catalysts (see Fig. S1), no vibration of nitrate at 1380–1390 cm^{-1} was observed [49]. According to this result, we believe that the NO_3^- ions were removed from the surface of these catalysts by the thoroughly washing during catalyst preparation. The disturbance of the residual NO_3^- can be excluded.

To get deeper insight of the acidity change during the preparation of PTNT, we also characterized the types of acid sites on the surfaces of TiO_2 P25, NaTNT and PTNT catalysts by FT-IR spectroscopy with pyridine as probe molecule. In a typical measurement, the sample was pressed to self-supporting tablet, loaded into a quartz IR cell with CaF_2 windows and evacuated at 423 K for 1 h to remove the physically absorbed water. After cooling down the IR cell to room temperature, the spectrum of sample was recorded by a mercury–cadmium–telluride (MCT) infrared detector as background. Subsequently, pyridine was introduced into the system and adsorbed on the catalyst for 30 min. The system was evacuated at room temperature for 40 min to remove the physically adsorbed pyridine. Subsequently, the final IR spectrum was recorded at room temperature by the subtraction of background.

2.2.8. H_2–O_2 titration

The metal dispersions (defined as the ratio of surface nickel atoms to total amount of nickel atoms in each catalyst) of the Ni catalysts were measured by H_2–O_2 titration with a micrometeritics autochem II 2920 automated catalyst characterization system. In a typical measurement, the sample was reduced in H_2 flow at 773 K for 2 h and purged in Ar flow at 783 K for 30 min to remove adsorbed H_2. After being cooled down to 393 K in Ar flow, the sample was purged with a 2 vol.% O_2/He flow for 30 min, and heated to 773 K in a constant Ar flow until the stabilization of baseline. Subsequently, the H_2 adsorption was conducted by dosage of 10 vol.% H_2/Ar pulse at 773 K. The metal dispersion of each Ni catalyst was calculated according to the amount of adsorbed H_2 and total Ni loading on the assumption that the molar ratio of H_2 to surface Ni atom is 1.5:1.

2.3. Activity tests

2.3.1. Hydroxyalkylation/alkylation (HAA) and alkylation of 2-MF

The HAA (or alkylation) reactions of 2-MF and the lignocellulosic carbonyl compounds were carried out in a round-bottom flask equipped with a reflux condenser and a magnetic stirrer according to the method described in our previous works [36–39]. Typically, 0.15 g catalyst, 3.28 g (40 mmol) 2-MF (for alkylation test, 1.64 g (20 mmol) 2-MF was used) and 20 mmol carbonyl compound were added to the flask and stirred for 4 h. The reaction temperature was controlled by a water bath. After the reactions, the HAA or alkylation products were analyzed by an Agilent 1100 high performance liquid chromatography (HPLC) equipped with a ZORBAX SB-C18 column (4.6 × 150 mm, 5 μm) and a refractive index detector (RID).

2.3.2. Hydrodeoxygenation (HDO)

The HDO of 5,5′-(butane-1,1-diyl) bis(2-methylfuran) (i.e. the 1a in Scheme 1) from the HAA of 2-MF and *n*-butanal was carried out at 533 K with a stainless steel tubular fixed-bed reactor described in

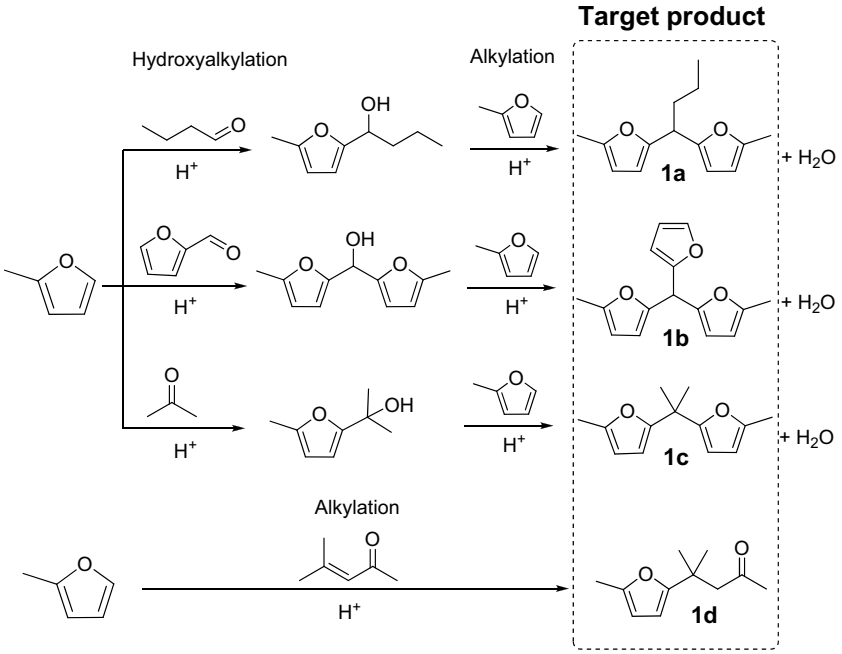

Scheme 1. Reaction pathways for the production of diesel precursors by the hydroxyalkylation/alkylation (HAA) or the alkylation of 2-MF and lignocellulosic carbonyl compounds. 1a: 5,5′-(butane-1,1-diyl) bis(2-methylfuran); 1b: 5,5′-(furan-2-ylmethylene) bis(2-methylfuran); 1c: 5,5′-(propane-2,2-diyl) bis (2-methylfuran); 1d: 4-methyl-4-(5-methylfuran-2-yl) pentan-2-one.

our previous work [36–38,50]. In each test, 1.80 g catalyst was used. Before the HDO reaction, the catalysts were reduced by hydrogen flow at 773 K for 2 h. The 1a (pre-purified by the two-step vacuum distillation (described in supporting information) of the HAA product of 2-MF and *n*-butanal) was fed into the reactor (at a rate of 0.04 mL min^{-1}) from the bottom of the reactor by a HPLC pump, together with a hydrogen flow (at the rate of 120 mL min^{-1}). The system pressure was controlled at 6 MPa by a back-pressure regulator. After passing through the tubular reactor, the HDO products were cooled down to room temperature and become two phases in a gas-liquid separator. The gaseous products were analyzed online by an Agilent 6890 N gas chromatograph. The liquid products were drained periodically and analyzed by another Agilent 7890 A gas chromatograph. The detail information about the calculation of carbon yields in the HDO step was described in the supporting information.

3. Results and discussion

3.1. Characterization

3.1.1. TEM images

From the TEM images of the titanate catalysts illustrated in Fig. 1, we can see that the TiO_2 P25 sample was composed of small nano particles (Fig. 1a). After the hydrothermal treatment with NaOH solution under different conditions and the ion-exchange with 0.1 mol L^{-1} HNO_3 solution, it was completely converted to titanates with nanotube (Fig. 1c) or nanowire (Fig. 1d) structures. According to literatures, these morphologic transformations follow a dissolution–reprecipitation mechanism [51]. In contrast, the PLT sample produced by the thermal treatment of TiO_2 P25 with Na_2CO_3 and the ion-exchange with acid solution exists as layered structure (Fig. 1e).

Fig. 2 shows the TEM images of Ni catalysts used in HDO process. According to the statistic results, the average sizes of Ni particles on different Ni catalysts were given in Table 1.

Table 1
Average sizes of Ni particles and the dispersions of Ni on different HDO catalysts measured by different methods.

Catalyst[a]	Average sizes of Ni particles (nm)		Metal dispersion (%)[b]
	XRD	TEM	
Ni/H-ZSM-5	13.8	12.9	9.0
Ni/H-MOR	25.2	22.4	4.8
Ni/H-β	12.3	12.2	14.7

[a] The theoretical content of Ni in each catalyst was 4 wt.%.
[b] The dispersion of Ni on catalyst was measured by H_2—O_2 titration.

Table 2
Contents of sodium and titanium and the Na/Ti atomic ratios in the different titanate catalysts.

Catalyst[a]	Na (wt.%)	Ti (wt.%)	Na/Ti atomic ratio
NaTNT	9.6	40.7	0.49
PTNT	0	47.0	0
NaTNW	8.4	47.7	0.37
PTNW	1.3	42.7	0.06
NaLT	11.4	42.2	0.57
PLT	2.3	58.2	0.08

[a] NaTNT: Na-titanate nanotube obtained by the hydrothermal treatment of TiO_2 P25 with NaOH solution; PTNT: protonated titanate nanotube prepared by the ion-exchanged of NaTNT with HNO_3 solution; NaTNW: sodium titanate nanowire obtained by the hydrothermal treatment of TiO_2 P25 with NaOH solution; PTNW: protonated titanate nanowire prepared by the ion-exchanged of NaTNW with HNO_3 solution; NaLT: layered sodium titanate obtained by the treatment of TiO_2 P25 with Na_2CO_3; PLT: protonated layered titanate prepared by the ion-exchanged of NaLT with HCl solution.

3.1.2. ICP-AES analysis

From the ICP-AES analysis results (see Table 2) of the titanate catalysts, evident decrease of sodium content in the titanate catalysts was observed after the ion-exchange with acid solutions. The sodium content in PTNT is almost zero, which can be explained by the complete substitution of Na^+ ions by H^+ ions. In contrast, there are still some Na^+ ions in the NaTNW and NaLT. The harder

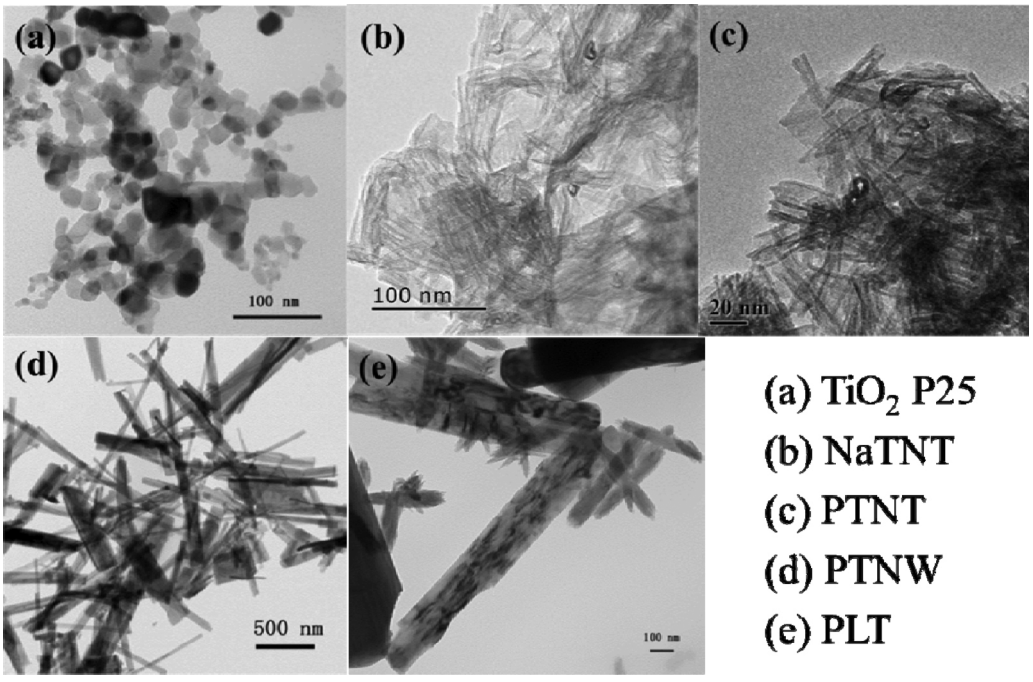

Fig. 1. TEM images of (a) TiO_2 P25, (b) sodium titanate nanotube (NaTNT), (c) protonated titanate nanotube (PTNT), (d) protonated titanate nanowire (PTNW) and (e) protonated layered titanate (PLT).

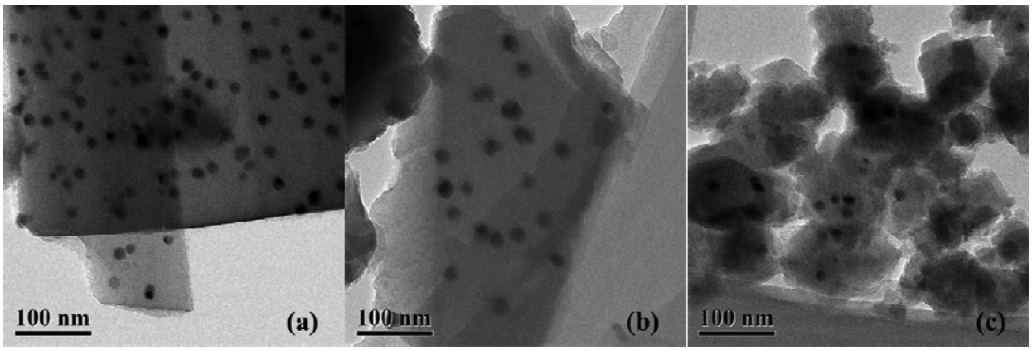

Fig. 2. TEM images of (a) Ni/H-ZSM-5, (b) Ni/H-MOR and (c) Ni/H-β after being reduced by hydrogen at 773 K for 2 h.

protonation of NaTNW and NaLT may be explained by their compact layer structures [52].

3.1.3. XRD patterns

From the XRD patterns of the titanate catalysts illustrated in Fig. 3, we can see that the TiO_2 P25 precursor is a mixture of anatase phase (JCPDS 84-1286) and rutile phase (JCPDS 4-0551). After the treatment with NaOH solution or Na_2CO_3, evident crystalline phase changes were observed.

According to literature [53], the NaTNT obtained by the hydrothermal treatment of P25 TiO_2 with 10 mol L^{-1} NaOH solution exists as $NaHTi_2O_4(OH)_2$ phase (JCPDS 31-1329). This result is also confirmed by the Na/Ti atomic ratio of NaTNT (0.49) according to the ICP-AES analysis. After ion-exchange with 0.1 mol L^{-1} HNO_3 solution, the peak at 10.2° disappeared. Meanwhile, the intensity of the peak at 28.4° decreased. These phenomena can be explained by the transformation from $NaHTi_2O_4(OH)_2$ phase to $H_2Ti_2O_4(OH)_2$ phase (JCPDS 47-0124) [53].

From the XRD patterns of LT samples, pure $Na_2Ti_3O_7$ (JCPDS 31-1329) was obtained by the calcination of Na_2CO_3 and TiO_2 P25 mixture at 1073 K. After ion-exchange with acid solution, the PLT sample as obtained mainly exists as $H_2Ti_3O_7$ phase (JCPDS 41-0192) [54,55]. These results were further verified by Na/Ti atomic ratio (0.57) in NaLT sample and the much lower sodium content in PLT according to ICP-AES analysis.

The NaTNW as-prepared was a mixture of $Na_2Ti_3O_7$ phase (JCPDS 31-1329) and anatase phase (JCPDS 84-1286). This attribution is also supported by the Na/Ti atomic ratio (0.37) in the sample. After ion-exchange with 0.1 M HNO_3, the PTNW as obtained is a mixture of layered or tunnel-structured $H_2Ti_nO_{2n+1}{\cdot}xH_2O$ phase [54], $Na_2Ti_6O_{13}$ phase (JCPDS 37-0951) and anatase phase (JCPDS 84-1286). This result was consistent with what we observed by the ICP analysis (Na/Ti ratio = 0.06)

Fig. 4 shows the XRD patterns of the Ni catalysts which have been reduced by hydrogen at 773 K for 2 h. From them, we can only see the peaks of metallic Ni and supports. According to Scherrer equation, the average sizes of Ni particles on Ni/H-ZSM-5, Ni/H-MOR and Ni/H-β catalysts were estimated as 13.8, 25.2 and 12.3 nm, respectively. These values are consistent with the statistic ones (12.9, 22.4 and 12.2 nm) based on the TEM results and the metal dispersions of the Ni catalysts (Ni/H-ZSM-5: 9.0%; Ni/H-MOR: 4.8% and Ni/H-β: 14.7%) which were measured by H_2—O_2 titration (see Table 1).

3.1.4. N_2 physical adsorption

From the results illustrated in Table 3, we can see that the transformation of TiO_2 P25 to NaTNT leads to the significant increase of its specific BET surface area (S_{BET}) (from 65 m^2 g^{-1} to 135 m^2 g^{-1}). This phenomenon can be explained by the nanotube structure of NaTNT formed by the hydrothermal treatment with NaOH solution (see Fig. 1b). The S_{BET} of NaTNT was further increased from 135 m^2 g^{-1} to 350 m^2 g^{-1} by the ion-exchange with acid solutions. This result can be rationalized by the larger pore volume of PTNT (0.79 mL g^{-1}) than that of NaTNT (0.21 mL g^{-1}). In contrast, it was noticed that the PLT and PTNW have even lower surface areas (56 m^2 g^{-1} and 42 m^2 g^{-1}) than that of TiO_2 P25 (65 m^2 g^{-1}), which can be explained by their solid structure (see TEM images shown in Fig. 1d and e).

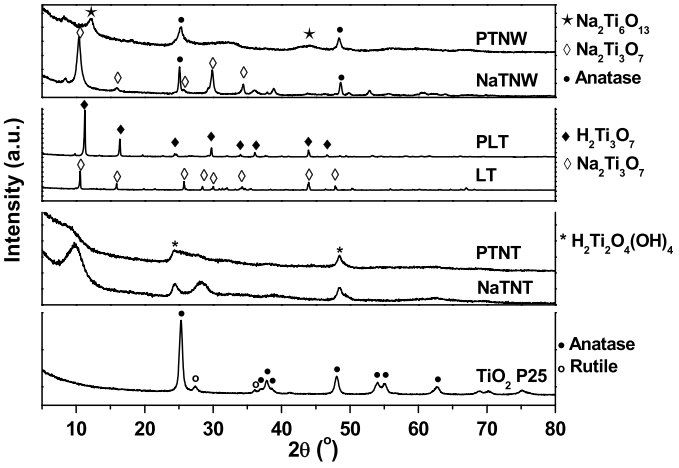

Fig. 3. XRD patterns of different titanate catalysts.

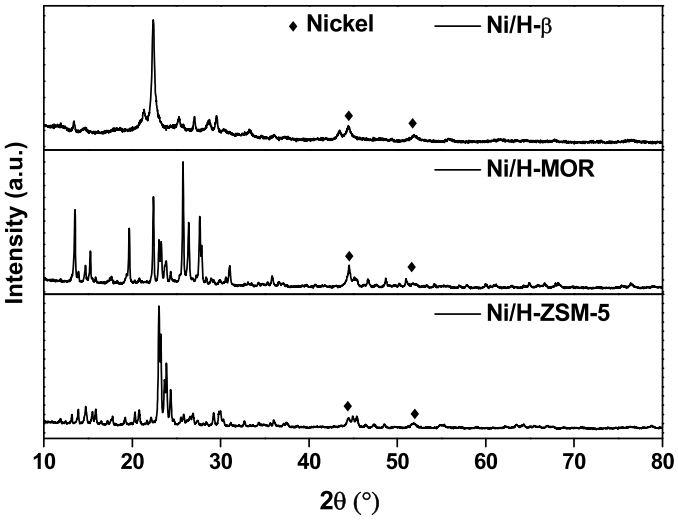

Fig. 4. XRD patterns of different Ni catalysts after being reduced by hydrogen at 773 K for 2 h.

Table 3
Properties of different titanate catalysts used in the HAA of 2-MF with *n*-butanal.

Catalyst[a]	S_{BET} ($m^2\,g^{-1}$)	Average pore size (nm)	Pore volume ($mL\,g^{-1}$)	Amount of acid site ($mmol\,g^{-1}$)[b]
TiO_2 P25	65	18.3	0.3	0.2
$PTiO_2$ P25	58	16.5	0.24	0.2
NaTNT	135	6.2	0.21	0.3
PTNT	350	7.5	0.79	1.1
PLT	56	8.6	0.11	0.1
PTNW	42	19.2	0.20	0.4

[a] $PTiO_2$ P25: protonated TiO_2 P25; NaTNT: Na-titanate nanotube obtained by the hydrothermal treatment of TiO_2 P25 with NaOH solution; PTNT: protonated titanate nanotube prepared by the ion-exchanged of NaTNT with HNO_3 solution; PLT: protonated layered titanate; PTNW: protonated titanate nanowire.
[b] Measured by NH_3 chemisorption.

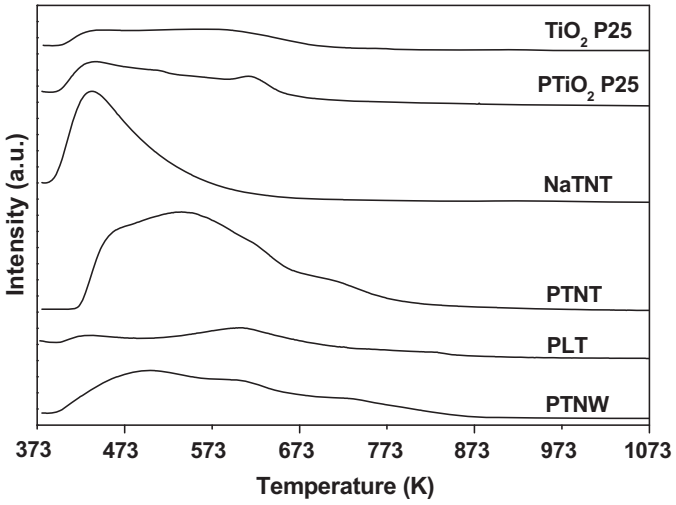

Fig. 5. NH_3–TPD profiles of different titanates.

3.1.5. NH_3–chemisorption and NH_3–TPD

From the results illustrated in Fig. 5 and Table 3, TiO_2 P25 and protonated TiO_2 P25 have weak acidity. Compared with them, the NaTNT has higher amount of acid sites (0.3 $mmol\,g^{-1}$ vs. 0.2 $mmol\,g^{-1}$). However, the strength of these acid sites is even lower than those over TiO_2 P25 (indicated by the lower NH_3 desorption temperature). After the ion-exchange with HNO_3 solution, the amount of acid sites on the surface of NaTNT increased significantly (from 0.3 $mmol\,g^{-1}$ to 1.1 $mmol\,g^{-1}$). Over the PTNT, evident NH_3 desorption at high temperature (>673 K) was observed. This can be attributed to the ammonia desorbed from the strong acid sites. In contrast, the acidities of PLT and PNW are very low. Only small amount of NH_3 desorption from PNW was observed at high temperature. From this result, we can see that the morphology of nanotube is crucial for the strong acidity of PTNT. According to literature [43,56–58], the strong acidity of PTNT can be explained by two reasons: (1) The acid sites in the H^+-exchanged titanate nanotube was generated by the hydroxyl groups on the scrolled titanate nanosheets. Although the acid strength of H^+-exchanged titanate is weak, the hydroxyl groups pointing towards the center of the nanotube may lead to a strong electric field which behaves as strong acid site. (2) The distortion in the rolled-up sheets of protonated titanate may also increase the acidity of the hydroxyl groups due to its high strain energy. This may be the reason for the small amount of strong acid sites over PTNW.

From the results demonstrated in Table 4, the sequence for the amount of acid sites over different zeolite supports is H-MOR (1.6 $mmol\,g^{-1}$) > H-ZSM-5 (1.15 $mmol\,g^{-1}$) > H-β (0.9 $mmol\,g^{-1}$). According to the temperature range for NH_3 desorbed from the surfaces of catalysts (see NH_3–TPD results shown in Fig. 6), same sequence was observed for acid strengths of these supports.

Table 4
Amounts of acid sites over different zeolite supports measured by NH_3 chemisorption.

Support	SiO_2/Al_2O_3 molar ratio	Acid amount ($mmol\,g^{-1}$)[a]
H-ZSM-5	25	1.15
H-MOR	24	1.60
H-β	25	0.90

[a] Measured by NH_3–chemsorption.

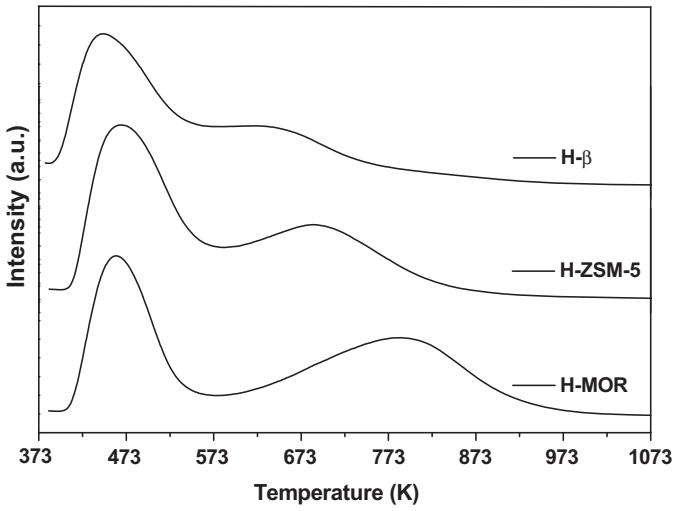

Fig. 6. NH_3–TPD profiles of different zeolite supports used in HDO tests.

3.1.6. FT-IR spectra with pyridine as probe molecule

From the FT-IR spectra of TiO_2 P25, NaTNT, PTNT catalysts after pyridine adsorption and evacuation at room temperature (see Fig. 7), evident bands at wavenumber of ~1445 cm^{-1} and ~1605 cm^{-1} can be observed for all three samples. According to literature [59], these bands can be attributed to Lewis acid sites generated by the surface coordinative unsaturated Ti^{4+} sites. Different with TiO_2 P25 and NaTNT, two broad bands at wavenumber of ~1540 cm^{-1} and ~1640 cm^{-1} were observed in the FT-IR

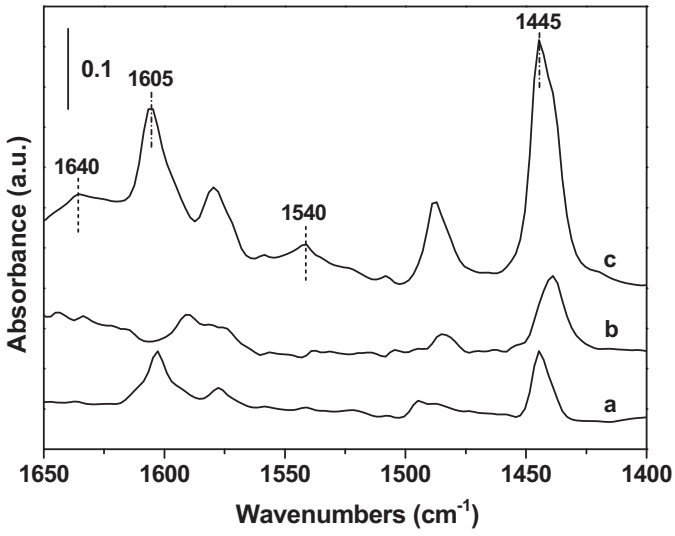

Fig. 7. FT-IR spectra of (a) TiO_2 P25, (b) NaTNT, (c) PTNT catalysts after pyridine adsorption and evacuation at room temperature.

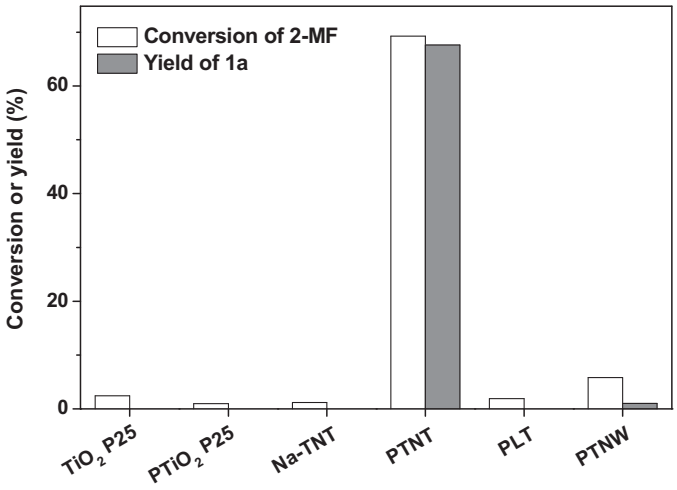

Fig. 8. Conversions of 2-MF (white bar) and the yields of 1a (grey bar) over different titania catalysts. Reaction conditions: 323 K, 4 h, 3.28 g (40 mmol) 2-MF, 1.44 g (20 mmol) *n*-butanal, 0.15 g catalyst.

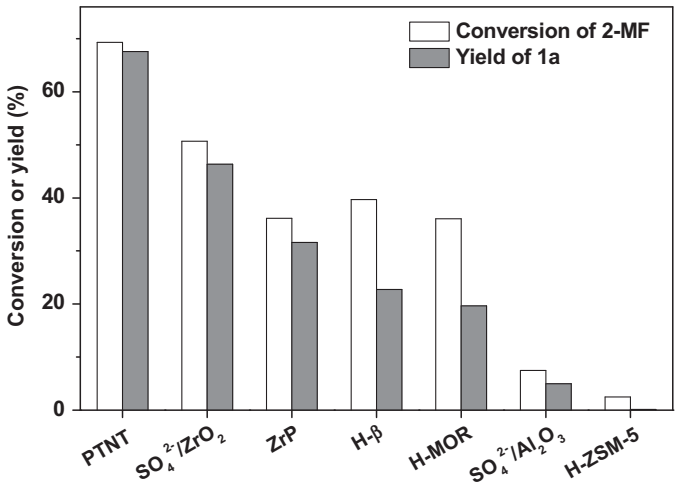

Fig. 9. Conversions of 2-MF (white bar) and the yields of 1a (grey bar) over different inorganic solid acid catalysts; reaction conditions: 323 K, 4 h, 3.28 g (40 mmol) 2-MF, 1.44 g (20 mmol) *n*-butanal, 0.15 g catalyst.

spectrum of PTNT. These bands are ascribed to the pyridine adsorbed on Brönsted acid sites [59]. From this result, we can see that the transformation of TiO_2 P25 to PTNT also leads to the generation of Brönsted acid sites which are absent on the surface of NaTNT and TiO_2 P25 catalysts. According to areas of the adsorption bands at ~1540 cm^{-1} and ~1445 cm^{-1}, the ratio of Brönsted acid to Lewis acid sites over the PTNT catalysts was estimated as 0.11 (see Table S1 in supporting information).

3.2. Activity tests

3.2.1. Hydroxyalkylation/alkylation (HAA)

Fig. 8 shows the catalytic performances of different titanates for the HAA of 2-MF and *n*-butanal (which can be obtained by the partial oxidization or dehydration of the *n*-butanol from the ABE fermentation of lignocellulose [22,60]). From it, we can see that TiO_2 P25, the protonated TiO_2 P25 ($PTiO_2$ P25) and NaTNT are inactive for the HAA of 2-MF. In contrast, the PTNT catalyst exhibited high activity for the HAA of 2-MF with *n*-butanal. Over such a catalyst, high yield (67.6%) of 5,5′-(butane-1,1-diyl) bis (2-methylfuran) (i.e. the 1a in Scheme 1) was achieved as the main product for the HAA of 2-MF with *n*-butanal (the HPLC chromatogram and NMR spectra of the liquid product were shown by Fig. S2 and Fig. S3 in supporting information). To investigate the effect of TiO_2 morphology, we also studied the catalytic performances of the protonated layered titanate (PLT) and the protonated titanate nanowire (PTNW). It was found that both catalysts were inactive for the HAA of 2-MF with *n*-butanal. The outstanding catalytic performance of PTNT for the HAA of 2-MF and *n*-butanal can be explained by following three reasons. (1) Higher specific surface area: according to the results of N_2−adsorption, it was found that the transformation of TiO_2 P25 to PTNT leads to the increasing of BET surface area, which is beneficial for the adsorption of reactants. (2) Higher acidity: from the results of NH_3 chemisorption and NH_3−TPD, we can see that the transformation of TiO_2 P25 to PTNT leads to the evident increase in the amount of acid sites and the generation of strong acid sites on the surface of catalyst. This may be another reason for the excellent performance of PTNT. According to literature [61] and our previous works [36–39], the HAA of 2-MF is very sensitive to the acid strength of catalysts. Strong acid is more active than weak acid for the HAA reactions of 2-MF. (3) Brönsted acid sites: from the FT-IR spectra with pyridine as probe molecule, the transformation of TiO_2 P25 to PTNT leads to the generation of Brönsted acid sites, which may be beneficial to the HAA reactions of 2-MF and *n*-butanal.

The activity of the PTNT for the HAA of 2-MF with *n*-butanal was compared with those of several often used inorganic solid acid materials (see Fig. 9). It was found that PTNT has the highest activity among the investigated catalysts. The activity advantage of PTNT is more evident at lower catalysts dosage (see Fig. S4 in supporting information). According to the yield of 1a at low catalyst dosage (in Fig. S4) and the amount of acid sites on the catalyst measured by NH_3 chemisorption, we calculated the turnover numbers (TON) of 2-MF to 1a over different catalysts. From the results shown in Fig. 10, the PTNT has the highest catalytic efficiency for the conversion of 2-MF to 1a, which is the reason for its higher activity even at low catalyst dosage.

Subsequently, we also explored the possibility to use PTNT as the catalyst for the HAA (or alkylation) of 2-MF with other lignocellulosic carbonyl compounds (such as furfural, acetone and mesityl oxide). The chemical structures and NMR spectra of the target products from the HAA (or alkylation) reactions were listed in Scheme 1 and Fig. S5–S7. As shown in Fig. 11, PTNT has good activity for the HAA (or alkylation) of 2-MF and other lignocellulosic carbonyl com-

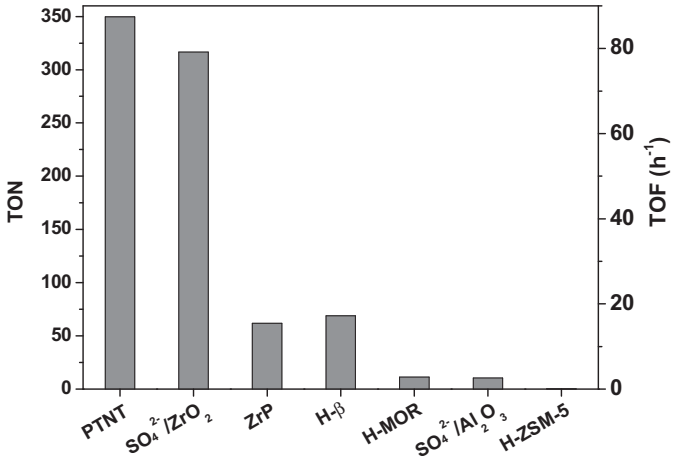

Fig. 10. TONs of 2-MF to 1a calculated based on the yields of 1a at low 2-MF conversions and the amounts of acid sites over different catalysts measured by NH_3 chemisorption. Reaction conditions: 323 K, 4 h, 3.28 g (40 mmol) 2-MF, 1.44 g *n*-butanal (20 mmol), 0.05 g catalyst.

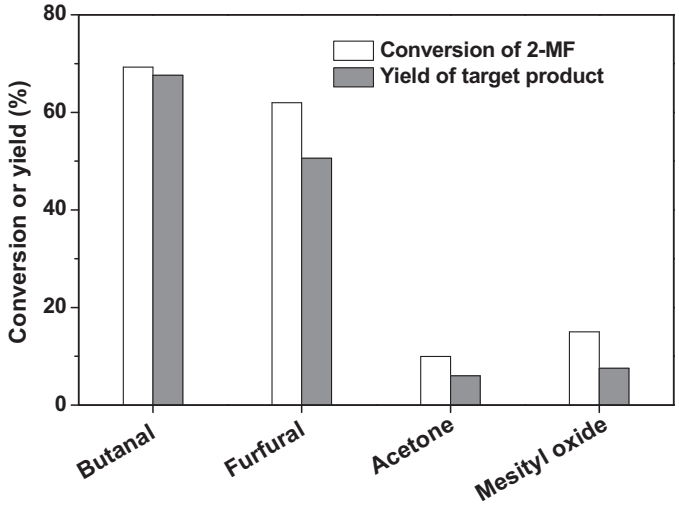

Fig. 11. Effect of carbonyl compound on the 2-MF conversion (white bar) and the yield of HAA (or alkylation) products (grey bar) over PTNT. Reaction conditions: 323 K, 4 h, 0.15 g catalyst, 40 mmol 2-MF, 20 mmol carbonyl compound (or 20 mmol 2-MF, 20 mmol mesityl oxide) were used for each reaction.

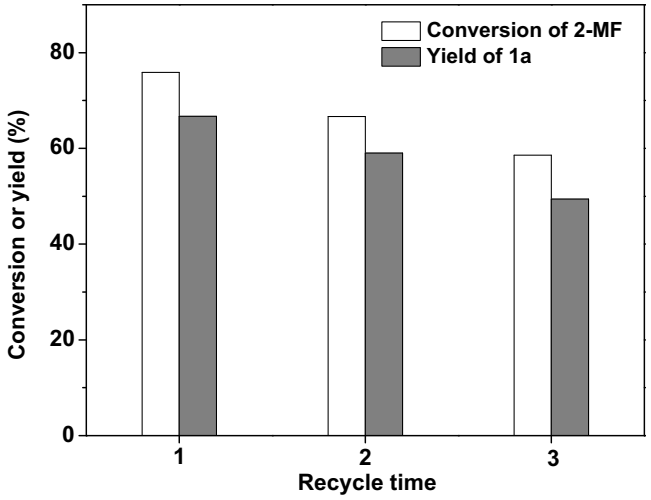

Fig. 12. 2-MF conversion (white bar) and 1a yield (grey bar) over PTNT catalyst as the function of recycle time. Reaction conditions: 323 K, 4 h, 3.28 g (40 mmol) 2-MF, 1.44 g (20 mmol) *n*-butanal, 0.15 g catalyst.

pounds. Over it, high yields of HAA (or alkylation) products can be achieved under mild conditions. From this result, we can see that the PTNT is a universal catalyst for the HAA reactions (or alkylation) of 2-MF. Among the carbonyl compounds investigated in this work, *n*-butanal exhibited the highest reactivity. This can be rationalized by the higher reactivity of aldehyde than ketone (or by the steric hindrance of furan group) [37].

Table 5 illustrated the effects of reaction temperature, reaction time and catalyst dosage on the 2-MF conversion and the 1a yield over PTNT. Under an optimized condition (0.15 g catalyst, 323 K and 8 h), 1a yield up to 77% was obtained over PTNT catalyst.

The stability of PTNT in the HAA of 2-MF and *n*-butanal was also studied. To do this, the PTNT catalyst was repeatedly used under the same reaction conditions. After each usage, the PTNT was filtrated, washed thoroughly with methanol (to remove the 1a and unreacted 2-MF or *n*-butanal) and evacuated at 333 K for 12 h. From Fig. 12, slight deactivation was observed over the PTNT catalyst. With the increase of recycle time, such a phenomenon becomes more evident. In order to check if the deactivation of PTNT is due to the water which was produced during the HAA reaction, we investigated the effect of water on the catalytic performance of PTNT. To do this, PTNT was added into water at the mass ratio of 0.15:1. The mixture was stirred at 323 K for 4 h (the same temperature and reaction time as we used in the HAA of 2-MF and *n*-butanal). After this pretreatment, the PTNT was separated from water by centrifugation, dried at 333 K for 12 h, and used in the HAA reaction. From the results shown in Fig. S8, no apparent difference was observed between the 2-MF conversions (or 1a yields) over the fresh and the water-treated PTNT, which means that the water has no evident influence on the catalytic performance of PTNT. To find out the reason for the deactivation of PTNT, we characterized the fresh and spent PTNT by N_2–adsorption, NH_3–TPD and TG-DTA-MS. According to the results shown in Table S2 and Fig. S9, evident decreases in the specific BET surface area (from 350 $m^2\ g^{-1}$ to 271 $m^2\ g^{-1}$), average pore size (from 7.5 nm to 4.2 nm), pore volume (from 0.79 mL g^{-1} to 0.57 mL g^{-1}) and the amount of acid sites (from 1.1 mmol g^{-1} to 1.0 mmol g^{-1}) were observed after the PTNT was used in the HAA of 2-MF and *n*-butanal for three times. From Fig. S10a, an exothermic peak around 611 K was observed in the TG-DTA profiles of the spent PTNT. According to the MS profile (see Fig. S10b), this peak can be attributed to the combustion of large polymeric molecules which were deposited on PTNT catalyst during the HAA of 2-MF and *n*-butanal. Analogous to what we have observed over Amberlyst resins [36,37], the generation of large polymeric molecules during the HAA reactions of 2-MF can block the pore and decrease the accessibility of acid sites on the surface of PTNT catalyst, which may be the intrinsic reason for the structure, acidity and activity changes of PTNT.

Table 5
Effects of reaction temperature, reaction time, catalyst dosage on the conversion of 2-MF and the yield of 1a over PTNT. Reaction conditions: 3.28 g (40 mmol) 2-MF and 1.44 g (20 mmol) *n*-butanal were used for each reaction.

Temperature (K)	Reaction time (h)	Catalyst mass (g)	Conversion of 2-MF (%)	Yield of 1a (%)
303	4	0.15	14.3	12.3
313	4	0.15	43.2	41.8
323	4	0.15	69.3	67.6
333	4	0.15	79.7	76.3
323	1	0.15	39.0	35.9
323	2	0.15	51.5	47.0
323	6	0.15	81.5	77.3
323	8	0.15	81.5	77.5
323	4	0.015	31.0	29.2
323	4	0.05	53.9	46.9
323	4	0.10	64.3	62.4
323	4	0.30	76.8	73.8

3.2.2. Hydrodeoxygenation (HDO)

As the final aim of this work, the HDO of 1a was carried out over H-ZSM-5, H-MOR and H-β loaded Ni catalysts under mild conditions (533 K, 6 MPa H_2). To facilitate the comparison, zeolites with similar SiO_2/Al_2O_3 molar ratio were used (see Table 4). From the analysis of the gas phase and liquid phase products by GC–MS, the 1a was completely converted to alkanes over Ni/H-ZSM-5 and Ni/H-MOR. However, the situation was different when Ni/H-β was used as catalyst. According to the chromatogram of the liquid products from the HDO of 1a over Ni/H-β (see Fig. S11 in supporting information), the peaks of oxygenates (or partial HDO species) were also observed. Therefore, we believe that the Ni/H-ZSM-5 and Ni/H-MOR are more active than Ni/H-β for the HDO of 1a. From the results shown in Fig. 13, higher carbon yield of diesel and jet fuel range alkanes (90%) was achieved over Ni/H-ZSM-5 than that over Ni/H-MOR (79%) under the same reaction conditions. At the same time, it was also noticed that the carbon yield of target product (i.e. 6-propyl-undecane) from the HDO of 1a over Ni/H-ZSM-5 is

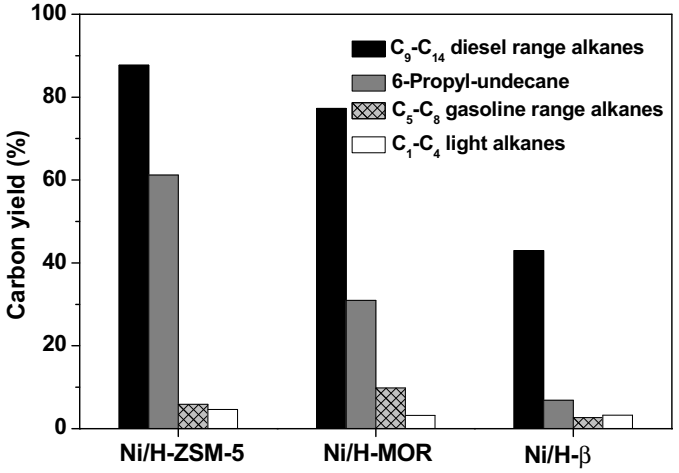

Fig. 13. Carbon yields of C_9—C_{14} diesel range alkanes (black bar), 6-propyl-undecane (grey bar), C_5—C_8 gasoline range alkane (light grey sparse bar) and C_1—C_4 light alkanes (white bar) from the HDO of 1a over different Ni catalysts. Reaction conditions: 533 K, 6 MPa, 1.8 g HDO catalyst; flow rate of liquid feedstock: 0.04 mL min^{-1} (WHSV = 1.3 h^{-1}); H_2 flow rate: 120 mL min^{-1}.

evidently higher than that over Ni/H-MOR. Therefore, the lower carbon yields of diesel and jet fuel range alkanes and 6-propyl-undecane over the Ni/H-MOR may be explained by the more serious hydrocracking and isomerization over this catalyst. This hypothesis was further confirmed by the higher carbon yields of pentane, nonane (the two major hydrocracking products as we reported previously [50]) and isomerized C_{14} alkanes over Ni/H-MOR (see Fig. 14).

In combination of characterization results, the different performances of Ni/H-β, Ni/H-ZSM-5 and Ni/H-MOR catalysts can be explained by following three reasons.

(1) Metal dispersion: according to results of XRD, TEM and H_2—O_2 titration, the average size of Ni particles on the Ni/H-MOR catalyst is evidently larger than those over Ni/H-ZSM-5 and Ni/H-β. This may be one reason for the higher carbon yield of shorter chain alkanes over this catalyst. According to literature [62], the larger metal particle size (or lower dispersion) will lead to the worse intimacy and balance of the acid and metal sites in the bifunctional catalyst, which favors the hydrogenolysis over metal sites or the cracking at the acid sites.

(2) Acidities of supports: according to the results of NH_3−chemisorption and NH_3−TPD, the H-ZSM-5 and H-MOR have higher amount of acid sites and higher acid strength (indicated by the higher NH_3 desorption temperature) than that of H-β. This may be one reason for the higher HDO activities of the Ni/H-ZSM-5 and Ni/H-MOR catalysts. In literature [63–66], it has been suggested that the strong acid sites are favorable for the HDO of biomass derived oxygenates from two aspects. (a) Strong acid sites are more active than weak acid sites for the dehydration [63]. In the previous work of Huber group [64], it was suggested that the dehydration followed by the hydrogenation is the major pathway for the C—O cleavage reaction. (b) Strong acid sites have higher activity for the ring-opening reaction of furan compounds which can facilitate the HDO of furan compounds [65]. In the recent work of Waidmann et al. [66], it was found that the ring-opening reaction (catalyzed by acid site) could greatly decrease the reaction temperature for the HDO of furan compounds to alkanes. According to their work, strong acid exhibited higher activity than weak acid for the catalytic ring-opening reaction. On the other hand, there is some balance for the metal sites and acid sites in the HDO of 1a. Too high acid strength and excess strong acid sites may lead to the side reactions of hydroisomerization and

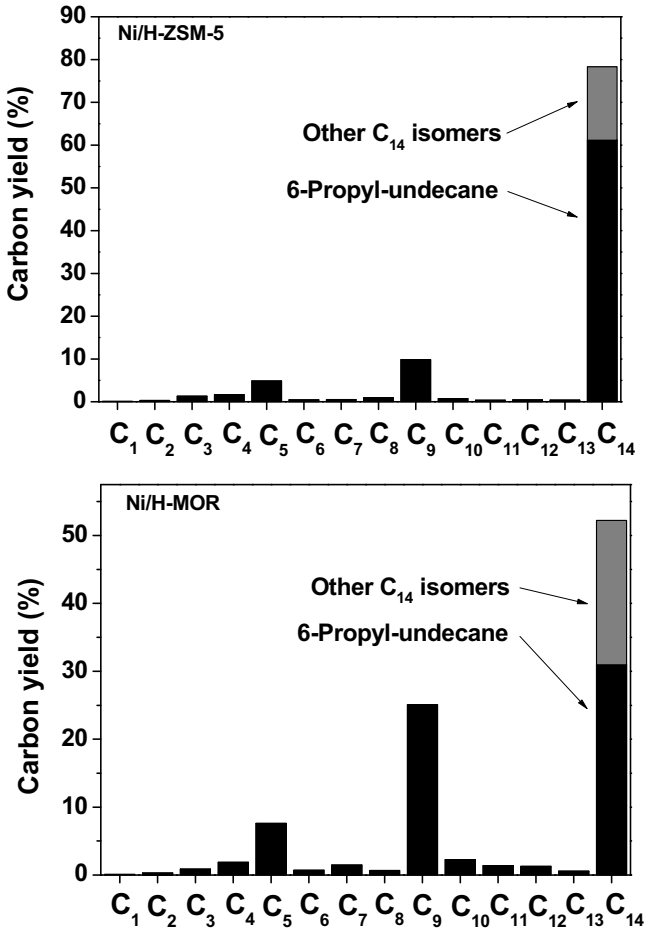

Fig. 14. Distributions of the alkanes obtained from the HDO of 1a over Ni/H-ZSM-5 and Ni/H-MOR. Reaction conditions: 533 K, 6 MPa H_2, 1.80 g catalyst; liquid feedstock flow rate of 0.04 mL min^{-1} (WHSV = 1.3 h^{-1}); H_2 flow rate of 120 mL min^{-1}.

hydrocracking. These reactions will decrease the carbon yields of 6-propyl-undecane and diesel and jet fuel range alkanes. From Fig. 6 and Table 4, it was noticed that the H-MOR has higher acid strength and higher amount of acid sites than H-ZSM-5. The

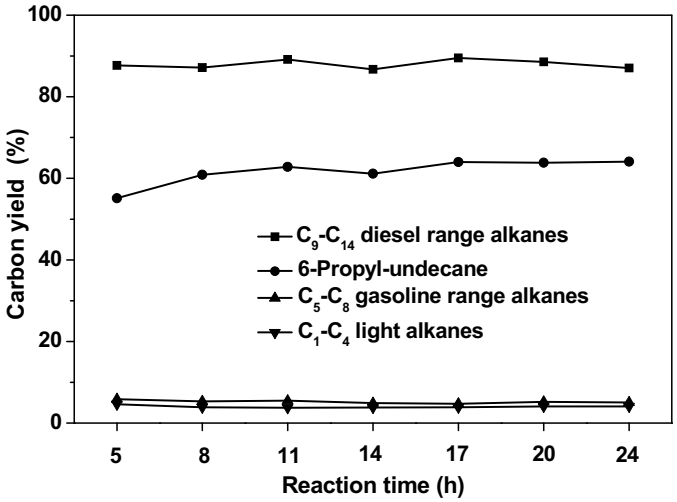

Fig. 15. Carbon yields of C_9—C_{14} diesel range alkanes (■), 6-propyl-undecane (●), C_5—C_8 gasoline range alkanes (▲) and C_1—C_4 light alkanes (▼) with time from the HDO of 1a over Ni/H-ZSM-5. Reaction conditions: 533 K, 6 MPa, 1.80 g Ni/H-ZSM-5 catalyst; liquid feedstock flow rate: 0.04 mL min^{-1} (WHSV = 1.3 h^{-1}); hydrogen flow rate: 120 mL min^{-1}.

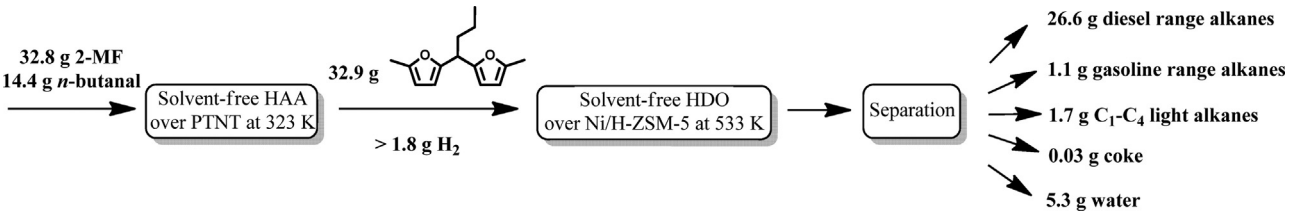

Fig. 16. Flow diagram for the production of renewable diesel and jet fuel range alkanes with 2-MF and *n*-butanal.

higher acid strength of H-MOR may be the reason for the higher carbon yield of C_{14} isomers over the Ni/H-MOR [67]. Moreover, the higher amount of strong acid sites of H-MOR support and the lower metal dispersion of Ni/H-MOR may lead to the more serious hydrocracking and lower carbon yield of diesel and jet fuel range alkanes over Ni/H-MOR [62,68].

(3) Pore size effect: from the structures of different zeolite supports illustrated in Fig. S12, H-ZSM-5 is the only structure with 10-membered pore openings. The smaller pore size makes it difficult for the alkane product to enter the framework of this zeolite. In consequence, isomerization is the lowest over Ni/H-ZSM-5. In contrast, the H-β structure has pores with 12 members in three dimensions whereas H-MOR has them only in one dimension. As the result, severer isomerization occurs over Ni/H-β and Ni/H-MOR than that over Ni/H-ZSM-5.

Finally, we studied the stability of Ni/H-ZSM-5 in the HDO of 1a. The experiment was carried out under the same reaction conditions (533 K and 6 MPa) as we used for the activity comparison. As shown in Fig. 15, the carbon yield of diesel and jet fuel range alkanes over Ni/H-ZSM-5 remained constant (at ~90%) during the 24 h continuous test, indicating that this catalyst is stable under the investigated conditions. From the TG-DTA-MS profiles of the spent Ni/H-ZSM-5 catalyst (see Fig. S13 in supporting information), two exothermic peaks at 530 K and 626 K were observed. According to the MS result (see Fig. S13b), the exothermic peak at 530 K can be attributed to the combustion of oxygenates which were strongly adsorbed on the Ni/H-ZSM-5 catalyst (confirmed by the simultaneous production of H_2O and CO_2), while the exothermic peak at 626 K may be attributed to the combustion of coke generated during the HDO process (because only CO_2 was identified as the combustion product). From Fig. S13a, the coke only accounts for 2.64 wt.% of the spent Ni/H-ZSM-5. According to this value, the overall carbon yield of coke during the 24-h continuous HDO test was estimated as 0.1%. Basing on the optimum results we obtained in this work, an input output diagram for the production of diesel and jet fuel range alkanes with 2-MF and *n*-butanal was proposed in Fig. 16.

4. Conclusions

Protonated titanate nanotube (PTNT) was proved to be an effective solid acid catalyst for the HAA of 2-MF with *n*-butanal. Compared with some often used inorganic solid acid catalysts, the PTNT has higher activity for the HAA of 2-MF with *n*-butanal. According to results of characterization, the transformation of TiO_2 P25 to PTNT by hydrothermal treatment with NaOH solution and ion-exchange with acid solution leads to (1) the evident increase in the specific BET surface area and the acidity (including the amount of acid sites and acid strength) of the catalyst, (2) the generation of Brönsted acid sites. All of these changes are responsible for the excellent performance of PTNT. The PTNT catalyst is also applicable to the HAA (or alkylation) of 2-MF and other lignocellulosic carbonyl compounds. The HAA product of 2-MF with *n*-butanal was hydrodeoxygenated over zeolites loaded Ni catalysts. Among them, the Ni/H-ZSM-5 demonstrated the highest HDO activity and selectivity to diesel and jet fuel range alkanes. During the long-time test, the Ni/H-ZSM-5 catalyst also exhibited good stability in the HDO process, which makes it a promising catalyst in the future application.

Acknowledgments

This work is supported by the Natural Science Foundation of China (No. 21106143; 21277140; 21173218; 21206160), 100-talent project of Dalian Institute of Chemical Physics (DICP) and the Independent Innovation Foundation of State Key Laboratory of Catalysis (No. R201113).

Appendix A. Supplementary data

Supplementary data associated with this article can be found, in the online version, at http://dx.doi.org/10.1016/j.apcatb.2015.01.022.

References

[1] G.W. Huber, S. Iborra, A. Corma, Chem. Rev. 106 (2006) 4044–4098.
[2] D.M. Alonso, S.G. Wettstein, J.A. Dumesic, Chem. Soc. Rev. 41 (2012) 8075–8098.
[3] T.D. Matson, K. Barta, A.V. Iretskii, P.C. Ford, J. Am. Chem. Soc. 133 (2011) 14090–14097.
[4] J. Jae, W.Q. Zheng, R.F. Lobo, D.G. Vlachos, ChemSusChem 6 (2013) 1158–1162.
[5] X. Wang, R. Rinaldi, ChemSusChem 5 (2012) 1455–1466.
[6] J.Q. Bond, A.A. Upadhye, H. Olcay, G.A. Tompsett, J. Jae, R. Xing, D.M. Alonso, D. Wang, T. Zhang, R. Kumar, A. Foster, S.M. Sen, C.T. Maravelias, R. Malina, S.R.H. Barrett, R. Lobo, C.E. Wyman, J.A. Dumesic, G.W. Huber, Energy Environ. Sci. 7 (2014) 1500–1523.
[7] M. Mascal, S. Dutta, I. Gandarias, Angew. Chem. Int. Ed. 53 (2014) 1854–1857.
[8] A. Corma, S. Iborra, A. Velty, Chem. Rev. 107 (2007) 2411–2502.
[9] P. Gallezot, Chem. Soc. Rev. 41 (2012) 1538–1558.
[10] N. Ji, T. Zhang, M.Y. Zheng, A.Q. Wang, H. Wang, X.D. Wang, J.G.G. Chen, Angew. Chem. Int. Ed. 47 (2008) 8510–8513.
[11] K. Barta, T.D. Matson, M.L. Fettig, S.L. Scott, A.V. Iretskii, P.C. Ford, Green Chem. 12 (2010) 1640–1647.
[12] C.L. Williams, C.C. Chang, P. Do, N. Nikbin, S. Caratzoulas, D.G. Vlachos, R.F. Lobo, W. Fan, P.J. Dauenhauer, ACS Catal. 2 (2012) 935–939.
[13] E. Mahmoud, D.A. Watson, R.F. Lobo, Green Chem. 16 (2014) 167–175.
[14] X. Wang, R. Rinaldi, Energy Environ. Sci. 5 (2012) 8244–8260.
[15] M. Zheng, J. Pang, A. Wang, T. Zhang, Chin. J. Catal. 35 (2014) 602–613.
[16] Y.L. Wang, W.P. Deng, B.J. Wang, Q.H. Zhang, X.Y. Wan, Z.C. Tang, Y. Wang, C. Zhu, Z.X. Cao, G.C. Wang, H.L. Wan, Nat. Commun. 4 (2013) 2141.
[17] G.W. Huber, J.N. Chheda, C.J. Barrett, J.A. Dumesic, Science 308 (2005) 1446–1450.
[18] E.L. Kunkes, D.A. Simonetti, R.M. West, J.C. Serrano-Ruiz, C.A. Gartner, J.A. Dumesic, Science 322 (2008) 417–421.
[19] J.Q. Bond, D.M. Alonso, D. Wang, R.M. West, J.A. Dumesic, Science 327 (2010) 1110–1114.
[20] A. Corma, O. de la Torre, M. Renz, N. Villandier, Angew. Chem. Int. Ed. 50 (2011) 2375–2378.
[21] A. Corma, O. de la Torre, M. Renz, Energy Environ. Sci. 5 (2012) 6328–6344.
[22] A. Corma, O. de la Torre, M. Renz, ChemSusChem 4 (2011) 1574–1577.
[23] R. Xing, A.V. Subrahmanyam, H. Olcay, W. Qi, G.P. van Walsum, H. Pendse, G.W. Huber, Green Chem. 12 (2010) 1933–1946.
[24] H. Olcay, A.V. Subrahmanyam, R. Xing, J. Lajoie, J.A. Dumesic, G.W. Huber, Energy Environ. Sci. 6 (2013) 205–216.
[25] C. Zhao, Y. Kou, A.A. Lemonidou, X.B. Li, J.A. Lercher, Angew. Chem. Int. Ed. 48 (2009) 3987–3990.
[26] C. Zhao, D.M. Camaioni, J.A. Lercher, J. Catal. 288 (2012) 92–103.
[27] P. Anbarasan, Z.C. Baer, S. Sreekumar, E. Gross, J.B. Binder, H.W. Blanch, D.S. Clark, F.D. Toste, Nature 491 (2012) 235–239.
[28] B.G. Harvey, R.L. Quintana, Energy Environ. Sci. 3 (2010) 352–357.

[29] A.D. Sutton, F.D. Waldie, R.L. Wu, M. Schlaf, L.A. Silks, J.C. Gordon, Nature Chem. 5 (2013) 428–432.
[30] S. Crossley, J. Faria, M. Shen, D.E. Resasco, Science 327 (2010) 68–72.
[31] M.J. Climent, A. Corma, S. Iborra, Green Chem. 16 (2014) 516–547.
[32] J.-P. Lange, E. van der Heide, J. van Buijtenen, R. Price, ChemSusChem 5 (2012) 150–166.
[33] R.M. West, Z.Y. Liu, M. Peter, J.A. Dumesic, ChemSusChem 1 (2008) 417–424.
[34] R.M. West, Z.Y. Liu, M. Peter, C.A. Gartner, J.A. Dumesic, J. Mol. Catal. A Chem. 296 (2008) 18–27.
[35] J. Yang, N. Li, G. Li, W. Wang, A. Wang, X. Wang, Y. Cong, T. Zhang, ChemSusChem 6 (2013) 1149–1152.
[36] G. Li, N. Li, Z. Wang, C. Li, A. Wang, X. Wang, Y. Cong, T. Zhang, ChemSusChem 5 (2012) 1958–1966.
[37] G. Li, N. Li, J. Yang, A. Wang, X. Wang, Y. Cong, T. Zhang, Bioresour. Technol. 134 (2013) 66–72.
[38] G. Li, N. Li, S. Li, A. Wang, Y. Cong, X. Wang, T. Zhang, Chem. Commun. 49 (2013) 5727–5729.
[39] S. Li, N. Li, G. Li, A. Wang, Y. Cong, X. Wang, T. Zhang, Catal. Today 234 (2014) 91–99.
[40] T. Kasuga, M. Hiramatsu, A. Hoson, T. Sekino, K. Niihara, Adv. Mater. 11 (1999) 1307–1311.
[41] K. Shankar, J.I. Basham, N.K. Allam, O.K. Varghese, G.K. Mor, X. Feng, M. Paulose, J.A. Seabold, K.-S. Choi, C.A. Grimes, J. Phys. Chem. C 113 (2009) 6327–6359.
[42] P. Roy, S. Berger, P. Schmuki, Angew. Chem. Int. Ed. 50 (2011) 2904–2939.
[43] M. Kitano, K. Nakajima, J.N. Kondo, S. Hayashi, M. Hara, J. Am. Chem. Soc. 132 (2010) 6622–6623.
[44] W. Dong, A. Cogbill, T. Zhang, S. Ghosh, Z.R. Tian, J. Phys. Chem. B 110 (2006) 16819–16822.
[45] N. Li, A. Wang, J. Tang, X. Wang, D. Liang, T. Zhang, Appl. Catal. B Environ. 43 (2003) 195–201.
[46] N. Li, A.Q. Wang, L. Lin, X.D. Wang, L.L. Ren, T. Zhang, Appl. Catal. B Environ. 50 (2004) 1–7.
[47] Y. Kamiya, S. Sakata, Y. Yoshinaga, R. Ohnishi, T. Okuhara, Catal. Lett. 94 (2004) 45–47.
[48] J.F. Pang, A.Q. Wang, M.Y. Zheng, T. Zhang, Chem. Commun. 46 (2010) 6935–6937.
[49] S.P. Newman, W. Jones, J. Solid State Chem. 148 (1999) 26–40.
[50] G. Li, N. Li, J. Yang, L. Li, A. Wang, X. Wang, Y. Cong, T. Zhang, Green Chem. 16 (2014) 594–599.
[51] T. Vu, H. Au, L. Tran, T. Nguyen, T. Tran, M. Pham, M. Do, D. Nguyen, J. Mater. Sci. 49 (2014) 5617–5625.
[52] H. Zhang, X.P. Gao, G.R. Li, T.Y. Yan, H.Y. Zhu, Electrochim. Acta 53 (2008) 7061–7068.
[53] J. Yang, Z. Jin, X. Wang, W. Li, J. Zhang, S. Zhang, X. Guo, Z. Zhang, Dalton Trans. (2003) 3898–3901.
[54] A.R. Armstrong, G. Armstrong, J. Canales, P.G. Bruce, Angew. Chem. Int. Ed. 43 (2004) 2286–2288.
[55] J. Yang, D. Li, X. Wang, X. Yang, L. Lu, J. Mater. Sci. 38 (2003) 2907–2911.
[56] M. Hartmann, A. Pöppl, L. Kevan, J. Phys. Chem. 100 (1996) 9906–9910.
[57] T. Yamamoto, T. Tanaka, T. Funabiki, S. Yoshida, J. Phys. Chem. B 102 (1998) 5830–5839.
[58] M. Iwamoto, Y. Tanaka, N. Sawamura, S. Namba, J. Am. Chem. Soc. 125 (2003) 13032–13033.
[59] M. Kitano, E. Wada, K. Nakajima, S. Hayashi, S. Miyazaki, H. Kobayashi, M. Hara, Chem. Mater. 25 (2013) 385–393.
[60] B.G. Harvey, H.A. Meylemans, J. Chem. Technol. Biotechnol. 86 (2011) 2–9.
[61] I. Iovel, E. Lukevics, Chem. Heterocycl. Compd. 34 (1998) 1–12.
[62] E. Blomsma, J.A. Martens, P.A. Jacobs, J. Catal. 165 (1997) 241–248.
[63] J. Macht, R.T. Carr, E. Iglesia, J. Catal. 264 (2009) 54–66.
[64] N. Li, G.W. Huber, J. Catal. 270 (2010) 48–59.
[65] W. Xu, Q. Xia, Y. Zhang, Y. Guo, Y. Wang, G. Lu, ChemSusChem 4 (2011) 1758–1761.
[66] C.R. Waidmann, A.W. Pierpont, E.R. Batista, J.C. Gordon, R.L. Martin, L.A. Silks, R.M. West, R.L. Wu, Catal. Sci. Tech. 3 (2013) 106–115.
[67] J. Macht, R.T. Carr, E. Iglesia, J. Am. Chem. Soc. 131 (2009) 6554–6565.
[68] N. Batalha, L. Pinard, C. Bouchy, E. Guillon, M. Guisnet, J. Catal. 307 (2013) 122–131.